Accepted Manuscript

A family of manganese complexes containing heterocyclic-based ligands with cytotoxic properties

Jessica Castro, Ester Manrique, Marlon Bravo, Maria Vilanova, Antoni Benito, Xavier Fontrodona, Montserrat Rodríguez, Isabel Romero
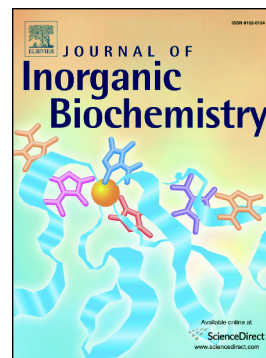
Please cite this article as: Jessica Castro, Ester Manrique, Marlon Bravo, Maria Vilanova, Antoni Benito, Xavier Fontrodona, Montserrat Rodríguez, Isabel Romero , A family of manganese complexes containing heterocyclic-based ligands with cytotoxic properties. The address for the corresponding author was captured as affiliation for all authors. Please check if appropriate. Jib(2017), https://doi.org/10.1016/j.jinorgbio.2018.01.021

This is a PDF file of an unedited manuscript that has been accepted for publication. As a service to our customers we are providing this early version of the manuscript. The manuscript will undergo copyediting, typesetting, and review of the resulting proof before it is published in its final form. Please note that during the production process errors may be discovered which could affect the content, and all legal disclaimers that apply to the journal pertain.

A family of manganese complexes containing heterocyclic-based ligands with cytotoxic properties

Jessica Castro,[b#] Ester Manrique,[a#] Marlon Bravo,[b] Maria Vilanova,*[b] Antoni Benito,[b] Xavier Fontrodona,[a] Montserrat Rodríguez*[a] and Isabel Romero*[a]

[a]Departament de Química and Serveis Tècnics de Recerca, Universitat de Girona, Campus de Montilivi, C/ Maria Aurèlia Capmany, 69, E-17003 Girona, Spain.

[b]Laboratori d'Enginyeria de Proteïnes, Departament de Biologia, Facultat de Ciències, Universitat de Girona, Campus de Montilivi, C/ Maria Aurèlia Capmany, 40, E-17003 Girona, Spain, and Institut d'Investigació Biomèdica de Girona Dr. Josep Trueta, Girona, Spain.

[#] J.C and E.C. equally contributed

* Corresponding authors e-mails: maria.vilanova@udg.edu, marisa.romero@udg.edu, montse.rodriguez@udg.edu. Fax number: int+34+972-418-150.

Abstract

We describe the synthesis of three new manganese (II) complexes containing the bidentate ligands 2-(1-methyl-3-pyrazolyl)pyridine (pypz-Me) and ethyl 2-(3-(pyridine-2-yl)-1H-pyrazol-1-yl)acetate (pypz-CH$_2$COOEt), with formula [MnX$_2$(pypz-Me)$_2$] (X = Cl$^-$ **1**, CF$_3$SO$_3^-$ **2**) and [Mn(CF$_3$SO$_3$)$_2$(pypz-CH$_2$COOEt)$_2$] **3**. Complexes **1-3** have been characterized through analytical, spectroscopic and electrochemical techniques, as well as by monocrystal X-ray diffraction analysis. The complexes show a six-coordinated Mn(II) ion though different stereoisomers have been isolated for the three compounds. Complexes **1-3**, together with the previously described compounds [MnCl$_2$(pypz-H)$_2$] **4**, [Mn(CF$_3$SO$_3$)$_2$(pypz-H)$_2$] **5**, [Mn(NO$_3$)$_2$(pypz-H)$_2$] **6**, [MnCl$_2$(H$_2$O)$_2$(pypz-H)$_2$] **7** (pypz-H= 2-(3-pyrazolyl)pyridine) and ([Mn(CF$_3$SO$_3$)$_2$((-)-L)$_2$] **8**, ((-)-L= (-)-pinene[5,6]bipyridine), were tested *in vitro* for cytotoxic activity against NCI-H460 and OVCAR-8 cancer cell lines. The geometry of a specific compound does not seem to influence its activity in a significant extent. However, among the tested compounds those that display hydrophobic substituents on the pyrazole ring and triflate ions as labile ligands show the best antiproliferative properties. Specifically, compound **8** containing the pinene-bipyridine ligand presents an antiproliferative activity similar to that of cisplatin and higher than that of carboplatin, and displays selectivity for tumour cells. Its antiproliferative effect is due to the generation of ROS species that allow the compound to interact with DNA.

Introduction

Transition-metal complexes with ligands containing nitrogen as donor atoms constitute an important class of coordination compounds that are able to perform a wide range of transformations.[1-9] Nitrogen-based ligands have well-known advantages such as chemical robustness or rich coordination chemistry in combination with inexpensive first-row transition metals.

The exponential development of bioinorganic chemistry along the last three decades has evidenced the key role of transition metals in biological processes and has manifested the unique properties they present for the design of new pharmaceutical drugs. In the specific field of chemotherapeutic agents for cancer treatment, *cis*-platin is a paradigmatic compound, which is nowadays used worldwide. However, its toxic side-effects have pushed on the research on alternative drugs, in some cases based on metals such as ruthenium, manganese, iridium, and copper.[10-15] Amongst these, manganese plays an important role in biological systems because it constitutes a co-factor for several enzymes such as manganese-containing superoxide dismutase (Mn-SOD), catalase, Mn-ribonucleotide reductase, and Mn-peroxidase.[16] Regarding its potential anticancer activity, it has been described that Mn(II) ions are mainly internalized in tumour cells through over-expressed transporters or receptors.[17] Moreover, Mn complexes have potentially fewer side effects and are more environment-friendly compared to platinum or ruthenium. Thus, complexes containing manganese may be valuable antitumor agents though they have been only

scarcely studied for such purpose.[18-24]

For metal-based drugs, the ligands may play important roles in target site recognition; the presence of a chelating ligand may control the reactivity toward different biomolecules (DNA, enzymes) and play a key role in the interaction with them through hydrogen bonding or intercalation. In addition, hydrophobicity may enhance cellular uptake. On the other hand, the coordination sites occupied by good leaving groups are labile sites for substitution reactions with target sites. Previously, we have studied the coordination of some nitrogen-based ligands such as pyridines,[25] bipyridines,[26,27] and pyrazoles[28] to manganese ions together with their characterisation and catalytic behaviour in epoxidation reactions. We thought that manganese complexes containing these N-chelating ligands and chloride, triflate or nitrate as labile ligands, could show good cytotoxicity against tumour cell lines as has been observed for the α-[Ru(azpy)$_2$Cl$_2$] compound, which contains the same type of ligands.[29] These manganese complexes would accomplish most of the aforementioned requirements for anticancer activity and then could be a promising alternative to the current "precious metal" based compounds. Moreover, slight modifications on the ligands such as alkylation at the acidic positions could enhance their hydrophobicity and inertness, thus, potentially improving their activity.

With all this in mind, in this work we describe the synthesis and full characterization of new Mn(II)-based compounds containing the pyrazolic ligands 2-(1-methyl-3-pyrazolyl)pyridine (pypz-Me) and ethyl 2-(3-(pyridine-2-yl)-1H-pyrazol-1-

yl)acetate (pypz–CH$_2$COOEt), Figure 1, together with chlorido or triflate as monodentate ligands. Compounds **1** and **2**, with general formula [MnX$_2$(pypz–Me)$_2$] (where X= Cl$^-$, **1** and X=CF$_3$SO$_3^-$, **2**), and **3** ([Mn(CF$_3$SO$_3$)$_2$(pypz–CH$_2$COOEt)$_2$]), have been prepared and tested as antitumor agents through the study of *in vitro* cytotoxicity tests against two human cancer cell lines, OVCAR–8 and NCI–H460. We have also tested other manganese compounds previously synthesized in our group (Figure 2), containing the bidentate 2–(3–pyrazolyl)pyridine (pypz–H) ligand (**4–7**),[28] and the chiral bidentate nitrogen ligand (–)–pinene[5,6]bipyridine ((–)–L), **8**.[26,27] The structure–activity relationships including factors such as the influence of N–R groups on the pyrazole ring or the geometrical isomer presented by a specific compound are discussed. The antiproliferative effect of compound **8** is of the same order of magnitude than that shown by cisplatin for both cell lines and even higher than that of carboplatin. We show that this compound inhibits the proliferation of cancer cells by triggering the generation of reactive oxygen species and by binding to DNA.

FIGURES 1 AND 2 HERE

Results and discussion

Synthesis, characterization and structure

The synthetic strategy followed for the preparation of Mn(II) complexes **1–3** is outlined in Scheme 1. Two different Mn(II) salts (manganese chloride or triflate) are used as starting materials and then the corresponding pypz–R ligand is added stepwise in a 2:1 ligand:metal ratio for the preparation of complexes. Complex [MnCl$_2$(pypz–Me)$_2$], **1**, is obtained in good yield from acetonitrile and colourless plates, suitable for X–ray diffraction, were crystallized from the mother liquor. Compounds [Mn(CF$_3$SO$_3$)$_2$(pypz–Me)$_2$], **2**, and [Mn(CF$_3$SO$_3$)$_2$(pypz–CH$_2$COOEt)$_2$], **3**, are obtained from Mn(CF$_3$SO$_3$)$_2$ by addition of the corresponding bidentate ligand in anhydrous THF. The three compounds have been characterized electrochemically as described in the SI (Figures S1 and S2).

SCHEME 1 HERE

The crystal structures of the three complexes have been solved by X–ray diffraction analysis. Crystallographic data and some additional structural parameters are presented in the SI (Tables S1 and S2, and Figure S3), whereas ORTEP plots with the corresponding atom labels for their X–ray structures are presented in Figure 3. Crystal structures of mononuclear compounds **1–3**, containing the pypz–Me and the

pypz−CH$_2$COOEt ligands, reveal in all cases a distorted octahedral geometry around the metal, where the Mn(II) ion is coordinated by four nitrogen atoms of two bidentate ligands and by two anionic monodentate ligands adopting a *cis* configuration.

The Mn−Cl and Mn−O$_{triflate}$, bond distances are comparable to those found in similar Mn(II) compounds.[30−35] Metal−ligand angles deviate significantly from the ideal value of 90º or 180º characteristic of a regular octahedron, due to the spatially constrained nature of the pypz−Me or pypz−CH$_2$COOEt ligands coordinated to the metal.

The spatial disposition of two pyrazolic ligands and two monodentate ligands in an octahedral environment, as is the case of complexes **1−3**, could potentially lead to a set of eight different isomers (including three pairs of enantiomers, see Figure S4 and the corresponding discussion in SI). It is noticeable that, as evidenced by the X−ray structures, complexes **1−3** are obtained as three different geometrical isomers (Figure 3): the *cis*−X−*trans*−py isomer for **1**, the *cis*−X−*cis*−(PyPz) for **2** and the *cis*−X−*trans*−pz isomer for **3**, where X represents the monodentate anionic ligands in each case. The analogous complexes **4−6** all containing the pypz−H ligand present the same isomer as compound **3**[28] whereas for complex **8,** containing triflate and the bipyridine−pinene ligand, a *cis*−X−*trans*−py isomer was found, although in this case no pyrazole rings are present in the structure of the ligands.[26]

FIGURE 3 HERE

Cytotoxicity assays

Before the cytotoxicity measurements, the stability of all the compounds in physiological conditions was tested by monitoring the changes in their UV-vis spectra along the time for a period of 72 h (Figure S5 displays representative spectra), and no significant changes from the initial spectrum were observed, thus indicating that the compounds are stable in PBS at pH 7.4. If the decoordination of N-donor ligands took place, we should expect a considerable drop in the absorbance due to the lower extinction coefficient of the free ligands with respect to the complexes (see experimental section).

The cytotoxic effect of the manganese compounds, containing pyridine-pyrazole (**1-7**) and (−)-pinene[5,6]bipyridine (**8**) ligands together with different monodentate labile ligands, was evaluated in two human cancer cell lines, NCI-H460 and OVCAR-8, after 72 h of exposure to them. Each ligand was also evaluated to discern the role of the manganese ion on the cytotoxic effect. All the tested compounds exhibited cytotoxic effects in a dose-dependent manner. Table 1 shows the IC_{50} values.

TABLE 1 HERE

Among the compounds containing pyridine-pyrazole ligands, **2** and **3** are cytotoxic for both cells lines, whereas none of the corresponding ligands displays significant activity. Compound **8** containing the pinene-bipyridine ligand (−)-L presents a

remarkable cytotoxicity that is of the same order of magnitude than that shown by cisplatin for both cell lines and between 10- and 22-fold higher than that of carboplatin for NCI-H460 and OVCAR-8, respectively (Table 1). In all cases manganese complexes have higher biological activity than their free ligands, confirming that the antitumor activities of pyrazole and bipyridine ligands can be enhanced by coordinating the corresponding ligand to manganese. In general, the NCI-H460 cell line is more sensitive to the action of compounds than the OVCAR-8 cell line.

Similar to other ruthenium[29] and platinum compounds,[36] the *cis*-coordinated labile groups in our complexes could be crucial for the good values obtained in the cytotoxic results, as it seems to be a key factor for the coordination of the metal to DNA[37] and the selectivity toward these bases appears to result from both electronic and steric effects.[38] The nature of N-R groups (CH_2COOEt, H or Me) seems also to be important in the activity shown by the different complexes with pyrazolic ligands. Thus, as a general trend, complexes containing the alkylated, less polar pypz-Me and pypz-CH_2COOEt ligands display better activities than those containing pypz-H. An additional influence of the N-R groups over the activity could arise from the potential H-bonding interactions that the R substituents on the pyrazole ring may present around the vacant site after removal of the leaving groups. If we compare, for instance, compounds **1-3**, we can observe that manganese compound **3**, which shows the *cis*-X-*trans*-pz geometry, places the two N-CH_2COOEt groups of the N-pyrazole ligands in *cis* to each monodentate labile

group, a fact that could favour a best accessibility or interaction through hydrogen bonding with some biomolecules approaching the vacant sites; in the case of complex **2**, only one N−CH$_3$ group is in *cis* to the labile positions and for complex **1** these N−CH$_3$ groups are situated in *trans*− to these groups, thus exerting low influence. Complexes **4−6** display the same *cis*−X−*trans*−pz geometry than complex **3** and, consequently, the geometrical isomer itself is not a determinant factor for cytotoxicity. Nevertheless, the geometry determines the spatial disposition of the N−R substituents which seems to be important in the antiproliferative activity of the pyrazolic complexes, with a certain contribution of the polarity of the substituents on the ligands as the more polar N−H groups instead of N−R organic substituents seem to slightly worsen the cytotoxic activity.

Compound **8**, which contains the more apolar ligand **(−)−L** and that presents pyridine rings in *cis* to the labile positions, exhibits increased activity. In concordance with the results obtained for the series of pyrazole ligands described above, we can assert that an overall increase in the hydrophobicity of the compounds seems to have certain importance since compounds **2** and **3**, and particularly **8**, exhibit the highest cytotoxic effect. However, an additional influence of the leaving group can be also postulated here, as these three compounds contain triflates as monodentate anionic ligands. The presence of triflate seems to have a positive influence on the cytotoxic activity when comparing for instance compounds **1** and **2**, with the chloro compound **1** displaying lower activity. This fact could be related to an easier dissociation of the triflate groups that could facilitate the coordination of the metal ion to target

molecules.

Taking into account the higher antiproliferative effect of compound **8**, and the remarkable difference with respect to the rest of the compounds containing pyrazole ligands, we further investigated its cytotoxicity on a panel of breast tumour cell lines as well as on non-tumour cells (Table 2). Compound **8** is twice more cytotoxic than its ligand on the three breast cancer cell lines representatives of tumours ER^+ PR^+ (MCF7), $Her2^+$ (SK-BR-3) and triple negative (MDA-MB-231). At the same time, it is clearly selective for cancer cells because its IC_{50} value for the non-tumour cells CC18-Co is higher than 30 µM.

TABLE 2 HERE

Provided the interesting results of compound **8** we further characterized how its antiproliferative effect may be exerted.

Analysis of the compound 8 treatment on the cell cycle phase distribution

We investigated by flow cytometry the effect of compound **8** on the OVCAR-8 and NCI-H460 cell cycle phase distribution. For comparison, the effect of its ligand was also analyzed. After 72 h of exposure to compound **8** or to its ligand, we observe only a minor accumulation on the G_0/G_1 cell cycle phase in both cells lines compared to untreated growing cells (Table 3).

TABLE 3 HERE

Compound 8 triggers ROS generation

To determine whether ROS play an important role in the antiproliferative effect induced by compound **8**, we investigated by flow cytometry whether the treatment with this compound increased the levels of ROS in OVCAR-8 and NCI-H460 cells. Cells were treated for 48 or 72 h with compound **8** at different concentrations and then labelled with carboxy-H_2DCFDA. For comparison, the effect of the ligand was also analyzed. As it is observed in Figure 4, the ROS levels increase with time and concentration in both cell lines either with the compound **8** or its ligand. The effect of compound **8** is higher than that of the ligand and in the NCI-H460 cell line, the ROS production is enhanced compared to OVCAR-8.

FIGURE 4 HERE

Further, we investigated whether the increase of ROS could explain the antiproliferative effect of compound **8**. We measured cellular viability, using the MTT assay, of NCI-H460 cell line treated with different concentrations of compound **8** or its ligand in the presence and absence of the reducing agent N-acetyl cysteine (NAC). This reducing agent counteracts the ROS production in the cells. Figure 5

shows that the presence of NAC reduces the antiproliferative effect of compound **8** at all the concentrations assayed. We also investigated whether compound **8** was able to generate ROS *in vitro* evaluating its ability to consume ascorbic acid. The results were negative (not shown) indicating that the compound *per se* does not produce ROS. This result seems to indicate that compound **8** increases intracellular ROS concentration by affecting those enzymes that control the homeostasis of ROS.

FIGURE 5 HERE

Binding of compound 8 to proteins and DNA

We tested the ability of compound **8** to interact with protein models and DNA. Protein interaction of compound **8** and its ligand was tested using three different protein models, chicken egg lysozyme, human pancreatic-ribonuclease and cytochrome C, following the changes in its UV-vis spectra after the addition of the protein at different times for a period of 48 h (metal/protein molar ratio 4/1). In any case the spectrum of compound **8** with its maximum at 292 nm was changed (Figure S6) indicating that it does not interact with these model proteins.

To test the ability of compound **8** and its ligand to interact with DNA, three different concentrations of the compound and its ligand were incubated with DNA (plasmid pUC18) at 37ºC for 24 h and the effects were analysed in an agarose gel electrophoresis. The results are shown in Figure 6A. As it can be observed, neither the ligand nor the compound are able to interact with DNA since at all the

concentrations assayed the bands observed corresponding to the supercoiled form (CCC) and circular nicked form (OC) are identical to those of the negative control (plasmid pUC18 alone). In contrast, cisplatin, the positive control, promotes the described effect on DNA i.e., the migration of the CCC form decreases until it co-migrates with relaxed (OC form) to reach the coalescence point.[39] Taking into account the results of ROS generation by compound **8** we performed the same assay of DNA interaction in the presence of H_2O_2. It can be observed (Figure 6B) that in the presence of H_2O_2, increasing concentrations of compound **8** from 25 to 75 μM are able to change the ratio of the CCC to OC form of DNA and at 75 μM concentration it is also observed the appearance of a band corresponding to the linear form of plasmid pUC18 (L) that it is formed when both DNA strands are broken. Finally, at 100 μM, degradation of DNA is clearly produced. In contrast, the ligand does not have any effect in the DNA topology even at the maximum concentration assayed when compared with the negative control (plasmid pUC18 alone). Thus, we can conclude that in the presence of ROS compound **8** cuts the DNA and promotes its degradation presenting a different behaviour from that observed for cisplatin in this assay. Provided that compound **8** and its ligand trigger ROS generation, the fact that the latter does not cut the DNA may explain the higher antiproliferative effect of the compound. This result confirms that metal ligand coordination enhances its cytotoxic properties.

FIGURE 6 HERE

Conclusions

We have synthesized and fully characterized a family of new Mn(II) complexes containing pyrazole-based ligands. The X-ray structures of complexes display hexacoordinated Mn(II) ions obtaining in all the cases different diastereoisomers. All compounds have been studied as potential antitumor agents, together with other previously described manganese complexes, containing pyrazole and bipyridine ligands.

Pyrazolic complexes **2** and **3**, and mainly the bipyridyl complex **8**, show antiproliferative activity against different human tumour cell lines. The overall hydrophobic nature of the compounds seems to be a determinant factor in their cytotoxic effect since complexes **2** and **3** (bearing the apolar -Me and -CH$_2$COOEt substituents at the bidentate ligands) and complex **8** (which contains the pinene-bipyridine ligand) are better than similar complexes which contain more polar pypz-H ligands. The geometrical isomer of the complexes is not itself a determinant factor on the cytotoxicity, but it may drive the spatial arrangement of the N-R substituents around the vacant sites after the decoordination of the leaving groups and thus induce favorable interactions with target molecules. The occurrence of triflate as monodentate anionic ligand, as is the case of complexes **2**, **3** and **8**, seems also to have a positive influence on the cytotoxic activity. Compound **8** displays a remarkable and selective antitumor activity which is of the same order of magnitude than cisplatin. This compound kills the cancer cells by generating ROS species that

enable it to cut the DNA. Therefore, we have identified a manganese compound that is a promising, economical and environment-friendly alternative to the present metal-based antitumor agents.

Experimental section

Materials

Unless otherwise indicated all reagents used in the present work were obtained from Aldrich Chemical Co and were used without further purification. Reagent grade organic solvents were obtained from SDS and high purity de-ionized water was obtained by passing distilled water through a nano-pure Milli-Q water purification system.

Instrumentation and measurements.

FT-IR spectra were taken in a Mattson-Galaxy Satellite FT-IR spectrophotometer containing a MKII Golden Gate Single Reflection ATR System. UV-Vis spectroscopy was performed on a Cary 50 Scan (Varian) UV-Vis spectrophotometer with 1 cm quartz cells. Cyclic voltammetric (CV) and differential pulse voltammetry (DPV) experiments were performed in an IJ-Cambria IH-660 potentiostat using a three electrode cell. Glassy carbon electrodes (3 mm diameter) from BAS were used as working electrode, a platinum wire as auxiliary and an $Ag/AgNO_3$ (10 mM) as the reference electrode. All cyclic voltammograms presented in this work were recorded under nitrogen atmosphere at a scan rate of 100 mV/s. The $E_{1/2}$ values were estimated from cyclic voltammetry as the average of the oxidative and reductive peak potentials $(E_{pa}+E_{pc})/2$ or directly from DPV waves. Unless explicitly mentioned the concentration of the complexes were approximately 1 mM. Elemental analyses were

performed using a CHNS-O Elemental Analyser EA-1108 from Fisons. ESI-MS experiments were performed on a Navigator LC/MS chromatograph from Thermo Quest Finnigan, using acetonitrile as a mobile phase.

X-ray structure determination.

Measurements of the crystals were performed on a Bruker Smart Apex CCD diffractometer using graphite-monochromated Mo Kα radiation (λ = 0.71073Å) from an X-Ray tube. Data collection, Smart V. 5.631 (BrukerAXS 1997-02); data reduction, Saint+ Version 6.36A (Bruker AXS 2001); absorption correction, SADABS version 2.10 (Bruker AXS 2001) and structure solution and refinement, structure solution and refinement, SHELXL-2013 (Sheldrick, 2013). The SQUEEZE tool in PLATON (Spek, A. L.,2009) was used to remove spurious electron density peaks in structure **2**, and disordered CH_2Cl_2 in structure **3**. The crystallographic data, as well as details of the structure solution and refinement procedures, are reported in Table S1. CCDC 1492238 (**1**), 1492239 (**2**), 1492240 (**3**), contain the supplementary crystallographic data for this paper. These data can be obtained free of charge from The Cambridge Crystallographic Data Centre via www.ccdc.cam.ac.uk/products/csd/request/

Preparations

The ligands 2-(1-Methyl-3-pyrazolyl)pyridine (pypz-Me)[40] and ethyl 2-(3-

-19-

(pyridine–2–yl)–1H–pyrazol–1–yl)acetate (pypz–CH$_2$COOEt),[41] and complexes Mn(CF$_3$SO$_3$),[42] **4–7**[28] and **8**[26] were prepared according to literature procedures. All synthetic manipulations were routinely performed under ambient conditions.

Synthesis of manganese complexes

Preparation of [MnCl$_2$(pypz–Me)$_2$] (1). To a solution of MnCl$_2$ (0.030 g, 0.236 mmol) in acetonitrile (5 mL), 0.072 g of pypz–Me (0.472 mmol) were added under stirring. The resulting white solution was stirred for 10 min and afterwards a white solid precipitated. This solid was filtered off, washed with diethyl ether and dried in air. Colourless plates, suitable for X–ray diffraction, were obtained from the mother liquor. Yield: 73.7 mg (70 %). Anal. Found (Calc.) for C$_{18}$H$_{19}$Cl$_2$N$_6$Mn: C, 47.93 (48.27); H, 3.70 (4.08); N, 18.65 (18.92) %. IR (cm^{-1}): υ = 3238–3142, 1604, 1431, 1241, 763. $E_{1/2}$ (CH$_3$CN + 0.1M n–Bu$_4$NPF$_6$, TBAH): 0.62 V. ESI–MS (m/z): 408 [MnCl(pypz–Me)$_2$]$^+$.

Preparation of [Mn(CF$_3$SO$_3$)$_2$(pypz–Me)$_2$] (2). 0.058 g (0.365 mmol) of pypz–Me were added under stirring to a solution of Mn(CF$_3$SO$_3$)$_2$ (0.064 g, 0.183 mmol) in anhydrous THF (5 mL). After 1 h a white precipitate was obtained and collected by filtration, washed thoroughly with diethyl ether and dried in vacuum. Colourless needles, suitable for X–ray diffraction, were grown by diffusion of ethyl ether into a THF solution of the compound. Yield: 70.2 mg (57 %). Anal. Found (Calc.) for C$_{20}$H$_{18}$F$_6$N$_6$O$_6$S$_2$Mn: C, 36.11 (35.78); H, 2.63 (2.70); N, 12.28 (12.52) %. IR (cm^{-1}):

υ = 3238–3142, 1608, 1437,1303, 1208, 1163, 1019, 773. $E_{1/2}$ (CH$_3$CN + 0.1M n–Bu$_4$NPF$_6$, TBAH): 0.76 V. ESI–MS (m/z): 522 [Mn(CF$_3$SO$_3$)(pypz–Me)$_2$]$^+$.

Preparation of [Mn(CF$_3$SO$_3$)$_2$(pypz–CH$_2$COOEt)$_2$], (3). 0.115 g (0.500 mmol) of pypz–CH$_2$COOEt were added under stirring to a solution of Mn(CF$_3$SO$_3$)$_2$ (0.088 g, 0.250 mmol) in anhydrous THF (5 mL). After 2 h, the volume was reduced to 1 mL and diethyl ether was added to obtain a white solid that was collected by filtration, washed thoroughly with diethyl ether and dried in air. Colourless needles, suitable for X–ray diffraction, were grown by diffusion of ethyl ether into a CH$_2$Cl$_2$ solution of the compound. Yield: 91.8 mg (45 %). Anal. Found (Calc.) for C$_{26}$H$_{26}$N$_6$F$_6$O$_{10}$S$_2$Mn·0.5 THF: C, 39.21 (39.49); H, 3.47 (3.55); N, 9.58 (9.87) %. IR (cm^{-1}): υ = 3122–2977, 1742, 1607, 1304, 1210, 1167, 1021, 780. $E_{1/2}$ (CH$_3$CN + 0.1M n–Bu$_4$NPF$_6$, TBAH): 0.80 V. ESI–MS (m/z): 666 [Mn(CF$_3$SO$_3$)(pypz–CH$_2$COOEt)$_2$]$^+$, 258.5 [Mn(pypz–CH$_2$COOEt)$_2$]$^{2+}$.

Cytotoxicity assays

Tested compounds

Compounds and their ligands were first reconstituted in DMSO and later diluted with sterile and bidistilled water to a final concentration of 4% DMSO and their concentration was determined using their extinction coefficients. The extinction coefficient of each compound was calculated experimentally by measuring their absorbance at the wavelength where each one presents its maximum (λ_{max}), i.e., 282 nm (for compound **1**), 248 nm (for compound **2**), 278 nm (for compounds **3** and **5**),

240 nm (for compound **4**), 276 nm (for compound **6**), 242 nm (for compound **7**), and

292 nm (for compound **8**), while for the ligands of compounds **1** to **3, 4** to **7**, and **8** we

used wavelengths of 278 nm, 276 nm, and 292 nm, respectively. A linear regression

equation between absorbance at λ_{max} (A_{max}) and different compound concentrations

was calculated. The extinction coefficients of compounds **1**, **2**, **3, 4**, **5**, **6**, **7,** and **8**

were 17526, 23274, 21380, 19082, 16291, 13353, 18186, and 23541 $M^{-1}cm^{-1}$,

respectively. For the ligands pypz–Me, pypz–CH_2COOEt, pypz–H, and (–)–L we

used extinction coefficients of 6719, 12452, 6717 and 15467 $M^{-1}cm^{-1}$, respectively.

Stock solutions were then diluted to the desired final concentrations with sterile

complete medium immediately before each experiment. Cisplatin (Pfizer, Spain) and

carboplatin (Teva, Spain) were included as controls in these experiments.

Cell lines and culture conditions

NCI–H460 human lung cancer and OVCAR–8 human ovarian cancer cell lines were

obtained from the National Cancer Institute–Frederick DCTD tumour cell line

repository. MCF7, MDA–MB–231 and SK–BR–3 human breast cancer cells lines and

CCD18–Co human colon fibroblasts were obtained from Celltec UB (Universitat de

Barcelona, Spain).

The NCI–H460, OVCAR–8, MCF7 and MDA–MB–231 cells were routinely grown in

RPMI, supplemented with 10% fetal bovine serum (FBS), 50 U/mL penicillin, 50

μg/mL streptomycin and 2 mM L-glutamine. The SK–BR–3 cells were grown in

McCoy's 5A medium and the CCD–18Co in DMEM, in both cases supplemented with

10% FBS, 50 U/mL penicillin, 50 μg/mL streptomycin and 2 mM L-glutamine. The cells were used immediately after thawing and were routinely grown at 37° C in a humidified atmosphere with 5% CO_2. All media and reagents used to culture the cell lines were from Lonza (Switzerland). Cells were maintained and propagated following established protocols and remained free of mycoplasma throughout the experiments.

Cell proliferation assays

Cells were seeded into 96-well plates at the appropriate density, i.e., 1,500 for OVCAR-8; 1,900 for NCI-H460; 4,000 for MCF7; 2,500 for MDA-MB-231; 10,000 for SK-BR-3 and 4,000 for CCD-18Co, cells per well. After 24 h of incubation, cells were treated for 72 h with various concentrations of the compounds. When indicated, the widely used ROS scavenger N-Acetyl-L-cysteine (NAC) (Sigma, St. Louis, MO, USA) was added to a final concentration of 5 mM. Cell viability was determined by the MTT method as previously described.[43] The IC_{50} value corresponds to the concentration of the assayed compound required to inhibit cell proliferation by 50% relative to untreated cells and, in each case, it was calculated by linear interpolation from the obtained growth curves. All data are reported as the mean $\pm$ standard error (SE) of at least three independent experiments with three replicates in each.

Cell cycle phase analysis

Cell cycle phase analysis was performed by propidium iodide (PI) staining. NCI-H460 and OVCAR-8 cells (400,000 cells/100-mm dish) were treated with compound **8** and

its ligand (2 μM or 9 μM for NCI-H460 and 5 μM or 24 μM for OVCAR-8) for 72 h. Cells were then harvested and fixed with 70% ethanol for at least 1 h at $-20°$C. Fixed cells were harvested by centrifugation and washed in cold PBS. These collected cells were resuspended in PBS (1-2 $\times$ 10^6/mL) and treated with RNase A (100 μg/mL) and PI (40 μg/mL) (Molecular Probes, Eugene, OR, USA) at $37°$C for 30 min prior to flow cytometric analysis. A minimum of 10,000 cells within the gated region were analyzed on a FACSCalibur flow cytometer (BD Biosciences, San Jose, CA, USA). Cell cycle distribution was analyzed using the FlowJo program (FreeStar, Ashland, OR, USA).

Flow cytometric analysis of ROS generation.

ROS generation was determined by flow cytometry using the carboxy-20, 70-dichlorodihydrofluorescein diacetate probe (carboxy-H_2DCFDA). Carboxy-H_2DCFDA is oxidized to green fluorescent dichlorofluorescein (DCF) by ROS species. Cells were seeded in 6-well plates (70,000 cells/well) in phenol red-free RPMI 24 h prior to treatments. Cells were treated with different concentrations of compound **8** and its ligand (2, 4.5 or 9 μM for NCI-H460 cells and 5, 12 or 24 μM for OVCAR-8 cells) for 48 or 72 h at $37°$C. After treatments, cells were washed with PBS and incubated with 1 μM carboxy-H_2DCFDA for NCI-H460 cells or 0.5 μM for OVCAR-8 cells in PBS for 30 min at 37ºC in the dark. Then, cells were collected with phenol red-free trypsin and analyzed on a FACSCalibur flow cytometer. The geometric mean fluorescence intensity of 10,000 cells was established using CellQuest Pro software (Becton Dickinson).

Spectrophotometric studies

Compound stability

Small amounts of freshly prepared individual compounds in 4% DMSO were diluted in PBS, pH 7.4. The concentration of each compound in the final sample was 10 µM. The resulting solutions were monitored by collecting spectra at 0, 24, 48 and 72 h at room temperature between 230 and 370 nm in a Perkin-Elmer Lambda BIO-20 UV-vis spectrophotometer.

In vitro ROS generation

Generation of ROS species *in vitro* was measured by consumption of ascorbic acid (AA). Small amounts of compound **8** and its ligand were dissolved in 4% DMSO and diluted to a final concentration of 1 µM with phosphate buffer pH 7.4. The reaction was initiated by the addition of a solution of AA to a final concentration of 100 µM. The disappearance of AA over time was followed by its UV absorbance at 265 nm using a Perkin-Elmer Lambda BIO-20 spectrophotometer.

Protein binding

UV-vis spectra (between 230 and 320 nm) using a Perkin-Elmer Lambda BIO-20 spectrophotometer of 25 µM of compound **8** and its ligand were recorded before and after the addition of each model protein (chicken egg lysozyme, human pancreatic-ribonuclease and cytochrome C) at a stoichiometric ratio of 4:1 (ligand or metal/protein) at different times for a period of 48 h in the dark in PBS pH 7.4.

DNA interaction analysis

DNA interaction was monitored by agarose gel electrophoresis. Stock solutions of the compound **8** and its ligand were freshly prepared in milliQ water with 4% DMSO. To investigate whether the presence of ROS could mediate the interaction of the compound with DNA, 1 µL of 30% H_2O_2 (w/v) was added to the reaction. The samples were prepared by mixing 0.5 μl of supercoiled pUC18 DNA at a concentration of 0.5 μg/μl (Thermo Scientific) with appropriate aliquots of the compound or ligand followed by dilution with TE buffer (10 mM Tris-HCl, pH 7.6, 1 mM EDTA) to a final volume of 20 μl. A sample of pUC18 DNA without neither compound nor ligand was used as negative control. The samples were then incubated at 37 °C for 24 h and then 4 µl of loading buffer (6x) (10 mM Tris-HCl, pH 7.6, 0.03% bromophenol blue, 0.03% xylene cyanol FF, 60% glycerol, 60 mM EDTA) were added to each sample. The mixed solutions were loaded on a 0.8% agarose gel in 0.5x TBE buffer (89 mM Tris-borate, pH 8.3, 2 mM EDTA,) and electrophoresis was carried out for 1 h and 10 min at 100 V. Gels were stained with ethidium bromide (1 µg/mL in TBE) for 15 min and the DNA bands were visualized under UV light. For comparison purposes, cisplatin effect was evaluated under the same experimental conditions.

Statistical analysis

All statistical analyses were performed with IBM SPSS Statistics 23 software for Windows (USA). Results were analysed using the Student's t test. P-values < 0.05 were considered statistically significant.

Acknowledgements

References

[1] D. C. Weatherburn, S. Mandal, S. Mukhopadhyay, S. Bhaduri and L. F. Lindoy, in: J. A. McCleverty and T. J. Meyer (Ed.), Comprehensive Coordination Chemistry II, Elsevier, Oxford, 2003, pp. 1–125.

[2] A. J. Wu, J. E. Penner-Hahn and V. L. Pecoraro, Chem. Rev. 104 (2004) 903–938.

[3] C. S. Mullins and V. L. Pecoraro, Coord. Chem. Rev. 252 (2008) 416–443.

[4] S. O. Kelley and J. K. Barton, Science 283 (1999) 375–381.

[5] D. B. Hall, R. E. Holmlin and J. K. Barton, Nature 382 (1996) 731–5.

[6] C. J. Burrows and J. G. Muller, Chem. Rev. 98 (1998) 1109–1152.

[7] S. C. Weatherly, I. V. Yang and H. H. Thorp, J. Am. Chem. Soc. 123 (2001) 1236–1237.

[8] S.-I. Murahashi, H. Takaya and T. Naota, Pure Appl. Chem. 74 (2002) 19–24.

[9] T. Naota, H. Takaya and S.-I. Murahashi, Chem. Rev. 98 (1998) 2599–2660.

[10] G. Gasser, I. Ott and N. Metzler-Nolte, J. Med. Chem. 54 (2011) 3–25.

[11] P. C. A. Bruijnincx and P. J. Sadler, Curr. Opin. Chem. Biol. 12 (2008) 197–206.

[12] A. M. Pizarro, A. Habtemariam and P. J. Sadler, Top. Organomet. Chem. (2010) 21–56.

[13] R. F. Brissos, A. Caubet and P. Gamez, Eur. J. Inorg. Chem. (2015) 2633–2645.

[14] J. Grau, R. F. Brissos, J. Salinas-Uber, A. B. Caballero, A. Caubet, O.Roubeau, L. Korrodi-Gregório, R. Pérez-Tomás and P. Gamez Dalton Trans. 44 (2015) 16061–16072.

[15] E. Wachter, A. Zamora, D. K. Heidary, J. Ruiz and E. C. Glazer, Chem. Commun. 52 (2016) 10121-10124.

[16] G. C. Dismukes, in: J. Reedijk (Ed.), Bioinorganic catalysis, Marcel Dekker, New York, 1993, pp. 317–346.

[17] M. Aschner, T. R. Guilarte, J. S. Schneider and W. Zheng, Toxicol. Appl. Pharmacol. 221 (2007) 131–147.

[18] K. I. Ansari, J. D. Grant, S. Kasiri, G. Woldemariam, B. Shrestha and S. S. Mandal, J. Inorg.

Biochem. 103 (2009) 818–826.

[19] M. X. Li, C. L. Chen, D. Zhang, J. Y. Niu and B. S. Ji, Eur. J. Med. Chem. 45 (2010) 3169–3177.

[20] D.-F. Zhou, Q.-Y. Chen, Y. Qi, H.-J. Fu, Z. Li, K.-D. Zhao and J. Gao, Inorg. Chem. 50 (2011) 6929–6937.

[21] F. Zhang, Q.-Y. Lin, X.-L. Zheng, L.-L. Zhang, Q. Yang and J.-Y. Gu, J. Fluoresc. 22 (2012) 1395–1406.

[22] S. K. Dash, S. Chattopadhyay, T. Ghosh, S. Tripathy, S. Das, D. Das and S. Roy, ISRN Oncol. (2013) Article ID 709269.

[23] T. A. Pereira, G. E. T. da Silva, R. B. Hernández, F. L. Forti and B. P. Espósito, Biometals 26 (2013) 439–446.

[24] J. Liu, W. Guo, J. Li, X. Li, J. Geng, Q. Chen and J. Gao, Int. J. Mol. Med. 35 (2015) 607–616.

[25] J. Rich, M. Rodríguez, I. Romero, X. Fontrodona, P. W. N. M. van Leeuwen, Z. Freixa, X. Sala, A. Poater and M. Solà, Eur. J. Inorg. Chem. (2013) 1213–1224.

[26] J. Rich, M. Rodríguez, I. Romero, L. Vaquer, X. Sala, A. Llobet, M. Corbella, M.-N. Collomb and X. Fontrodona, Dalton Trans. (2009) 8117–8126.

[27] J. Rich, E. Manrique, F. Molton, C. Duboc, M.-N. Collomb, M. Rodríguez and I. Romero, Eur. J. Inorg. Chem. (2014) 2663–2670.

[28] E. Manrique, A. Poater, X. Fontrodona, M. Solà, M. Rodríguez and I. Romero, Dalton Trans. 44 (2015) 17529-17543.

[29] A. H. Velders, H. Kooijman, A. L. Spek, J. G. Haasnoot, D. de Vos and J. Reedijk, Inorg. Chem. 39 (2000) 2966–2967.

[30] S. McCann, M. McCann, M. T. Casey, M. Jackman, M. Devereux and V. McKee, Inorg. Chim. Acta 279 (1998) 24–29.

[31] C. Chen, H. Zhu, D. Huang, T. Wen, Q. Liu, D. Liao and J. Cui, Inorg. Chim. Acta 320 (2001) 159–166.

[32] J. A. Smith, J.-R. Galán-Mascarós, R. Clérac, J.-S. Sun, X. Ouyang and K. R. Dunbar, Polyhedron 20 (2001) 1727–1734.

[33] C. Baffert, I. Romero, J. Pécaut, A. Llobet, A. Deronzier and M.-N. Collomb, Inorg. Chim. Acta 357 (2004) 3430–3436.

[34] R.-Q. Zou, C.-S. Liu, X.-S. Shi, X.-H. Bu and J. Ribas, CrystEngComm 7 (2005) 722-727.

[35] R. van Gorkum, F. Buda, H. Kooijman, A. L. Spek, E. Bouwman and J. Reedijk, Eur. J. Inorg. Chem. (2005) 2255–2261.

[36] O. Novakova, J. Kasparkova, O. Vrana, P. M. van Vliet, J. Reedijk and V. Brabec, Biochemistry 34 (1995) 12369–12378.

[37] A. C. G. Hotze, A. H. Velders, F. Ugozzoli, M. Biagini-Cingi, A. M. Manotti-Lanfredi, J. G. Haasnoot and J. Reedijk, Inorg. Chem. 39 (2000) 3838–3844.

[38] Z. Liu and P. J. Sadler, Acc. Chem. Res. 47 (2014) 1174–1185.

[39] P. N. Yadav, R. E. Beveridge, J. Blay, A. R. Boyd, M. W. Chojnacka, A. Decken, A. A. Deshpande, M. G. Gardiner, T. W. Hambley, M. J. Hughes, L. Jolly, J. A. Lavangie, T. D. MacInnis, S. A. McFarland, E. J. New and R. A. Gossage, Med. Chem. Commun. 2 (2011) 274.

[40] W. R. Thiel and J. Eppinger, Chem. Eur. J. 3 (1997) 696–705.

[41] M. Jia, A. Seifert and W. R. Thiel, Chem. Mater. 15 (2003) 2174–2180.

[42] Y. Inada, Y. Nakano, M. Inamo, M. Nomura and S. Funahashi, Inorg. Chem. 39 (2000) 4793–4801.

[43] J. Castro, M. Ribó, T. Puig, R. Colomer, M. Vilanova and A. Benito, Invest. New Drugs 30 (2012) 880–888.

Table 1. IC$_{50}$* values (μM) of tested ligands and compounds **1–8** on the indicated cell lines.

Compound	NCI–H460	OVCAR–8
[MnCl$_2$(pypz–Me)$_2$], 1	160.8±20.2	>600.0
[Mn(CF$_3$SO$_3$)$_2$(pypz–Me)$_2$], 2	94.3±10.9	318.3±53.0
[Mn(CF$_3$SO$_3$)$_2$(pypz–CH$_2$COOEt)$_2$], 3	51.3±7.2	212.5±37.5
[MnCl$_2$(pypz–H)$_2$], 4	124.7±2.6	373.1±62.7
[Mn(CF$_3$SO$_3$)$_2$(pypz–H)$_2$], 5	189.2±29.2	492.4± 93.4
[Mn(NO$_3$)$_2$(pypz–H)$_2$], 6	157.2±32.1	>600.0
[MnCl$_2$(H$_2$O)$_2$(pypz–H)], 7	132.2±23.5	413.1±45.8
[Mn(CF$_3$SO$_3$)$_2$((–)–L)$_2$], 8	1.7±0.4	4.7±0.4
(–)–L	3.3±0.1	15.9±3.8
pypz–Me	>600.0	>600.0
pypz–CH$_2$COOEt	160.5±21.3	>600.0
pypz–H	>600.0	>600.0
Cisplatin	1.0±0.1	6.9±1.2
Carboplatin	12.8±2.2	110.0±4.2

*IC50 values correspond to the concentrations of each compound or its ligands that are required to inhibit cell proliferation by 50%. Data are presented as mean ± SE of at least three independent experiments conducted in triplicate

Table 2. IC_{50}* values (μM) of compound **8** and its ligand on the indicated cell lines

Cell line	Compound 8	(−)−L
MCF7	5.4±0.4	11.9±1.9
MDA−MB−231	7.5±1.1	15.5±0.3
SK−BR−3	15.1±1.6	27.1±1.7
CCD−18Co	>30.0	>30.0

*$IC50$ values correspond to the concentrations of each compound or its ligands that are required to inhibit cell proliferation by 50%. Data are presented as mean ± SE of at least three independent experiments conducted in triplicate

Table 3. Effects of compound **8** and its ligand at the indicated concentrations on the OVCAR–8 and NCI–H460 cell cycle phase distribution after treatment for 72 h. Untreated OVCAR–8 and NCI–H460 cells were used as control.

OVCAR–8*	Control	Compound 8		(–)–L	
		5 µM	24 µM	5 µM	24 µM
G0/G1	52.9	58.2	64.7	58.8	63.6
S	30.1	27.3	21.5	27.0	24.0
G2/M	15.8	14.1	11.8	13.5	10.9

NCI–H460*	Control	Compound 8		(–)–L	
		2 µM	9 µM	2 µM	9 µM
G0/G1	65.7	62.4	72.2	60.9	71.5
S	20.6	22.1	16.8	25.4	18.4
G2/M	13.8	15.3	10.4	13.6	9.8

*Treated cells were permeabilized and stained with PI. Cell DNA content was analyzed by flow cytometry. Data are representative of three independent assays. Values were analyzed from 10,000 total events

FIGURES AND SCHEME CAPTIONS.

Scheme 1. Synthetic strategy followed for the synthesis of complexes **1-3**.

Figure 1. Drawing of the pinene-bipyridine and pyrazolic ligands.

Figure 2. Schematic drawing of complexes **4-8**.

Figure 3. ORTEP plots and labelling schemes for the corresponding heteroatoms (left), and schematic representation of the diastereisomer obtained (right) for compounds **1-3**.

Figure 4. ROS production triggered by compound **8** and its ligand in OVCAR-8 (A) and NCI-H460 (B) cell lines. Cells were treated for 48 and 72 h with the compound or (-)-L and generation of ROS was measured by flow cytometry after labelling with carboxy-H_2DCFDA (see the text for more details). ROS levels are indicated as fold-increase vs control (non-treated cells). Values were analyzed from 10,000 total events. Data are presented as mean $\pm$ SE of at least three independent experiments. Differences versus untreated control cells were considered significant at *$p < 0.05$.

Figure 5. Cellular viability of NCI-H460 cells after treatment with compound **8** and

its ligand in the presence and absence of N-acetyl cysteine (NAC). Cellular viability was measured by the MTT assay. Data are presented as mean $\pm$ SE of at least three independent experiments. Differences in the cell viability values of cells with and without NAC treatment were considered significant at *p < 0.05.

Figure 6. Agarose gel electrophoresis of pUC18 plasmid DNA treated with different concentrations (indicated in μM) of compound **8** and its ligand in the absence (A) and presence of H_2O_2 (B). (A) From left to right, lane 1, cisplatin (positive control), lane 2 plasmid pUC18 alone (negative control), lanes 3-6 increasing amounts of compound **8** and lanes 7-10 increasing amounts of its ligand ((-)-L); (B) From left to right in both gels, lane 1 cisplatin (positive control), lane 2 plasmid pUC18 alone (negative control), lanes 3-6 increasing amounts of compound **8** or its ligand ((-)-L). OC = open circular form; CCC = covalently closed circular form; L = linear form.

Scheme 1.

X = Cl
CH$_3$CN → [MnCl$_2$(pypz-Me)$_2$], **1**

X = CF$_3$SO$_3$ → [Mn(CF$_3$SO$_3$)$_2$(pypz-Me)$_2$], **2**

THF → [Mn(CF$_3$SO$_3$)$_2$(pypz-CH$_2$COOEt)$_2$], **3**

MnX$_2$

pypz-R : Mn
2:1

pypz-R

R = CH$_3$ or CH$_2$COOEt

Figure 1.

pypz-Me

pypz-CH$_2$COOEt

pypz-H

(-)-L

Figure 2.

X: Cl, **4**
CF$_3$SO$_3$, **5**
NO$_3$, **6**

7
(mixture of isomers *a* and *b*)

7a   *7b*

8

Figure 3.

1

cis-X-*trans*-Py

2

cis-X-*cis*-(PyPz)

3

*cis*-X-*trans*-Pz
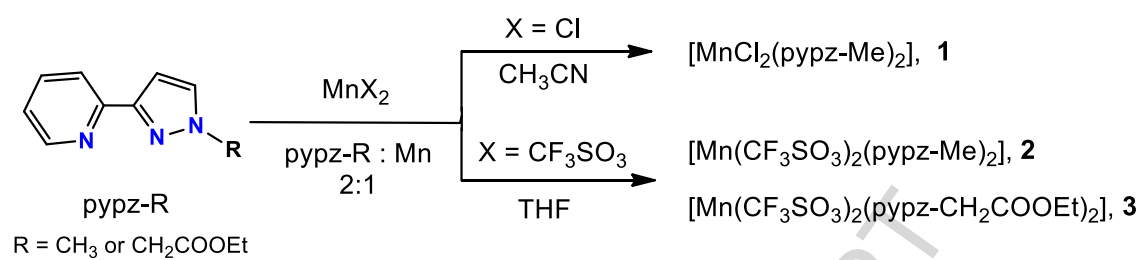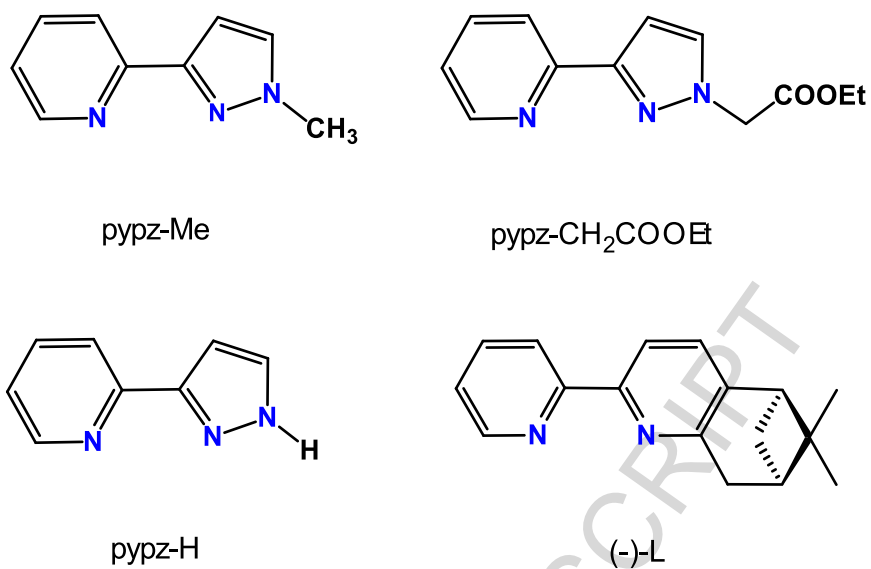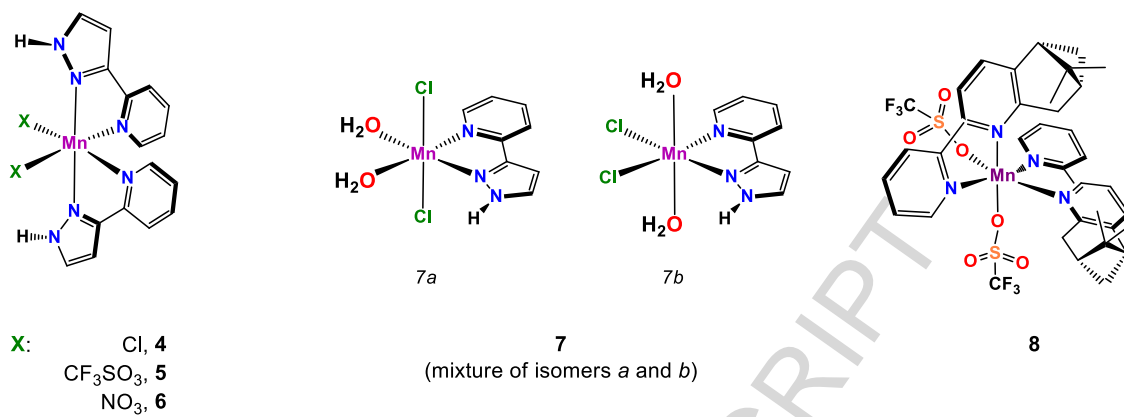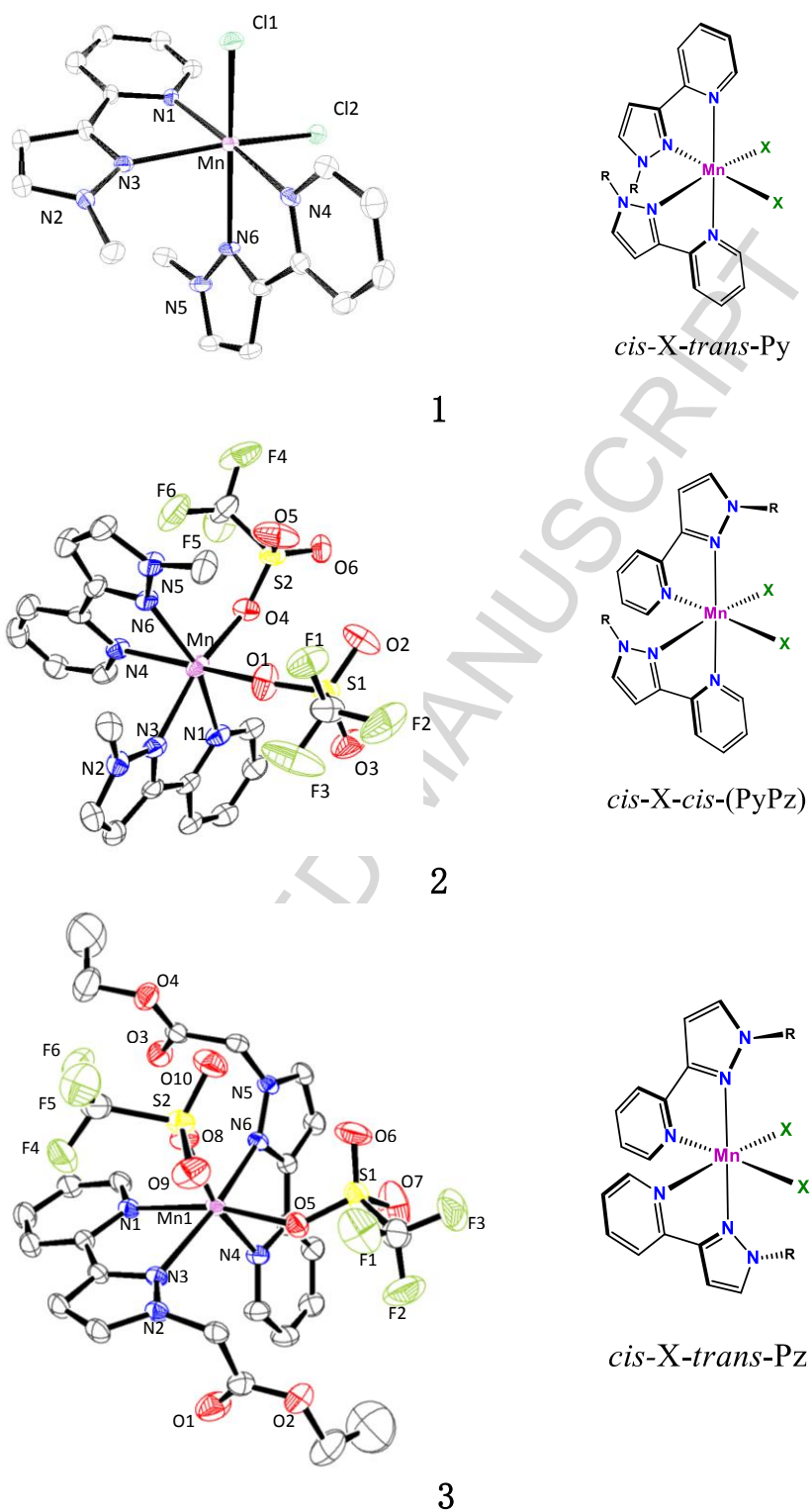
Figure 4.

(A) OVCAR-8


(B) NCI-H460

Figure 5.

Figure6.

A

B
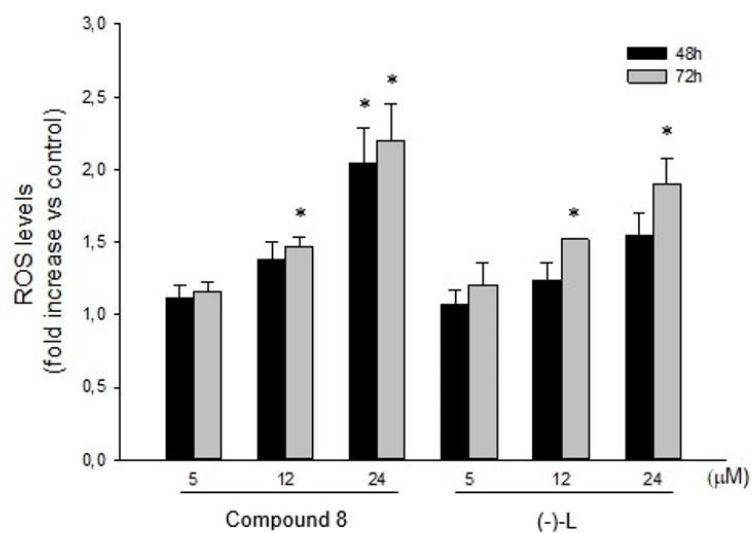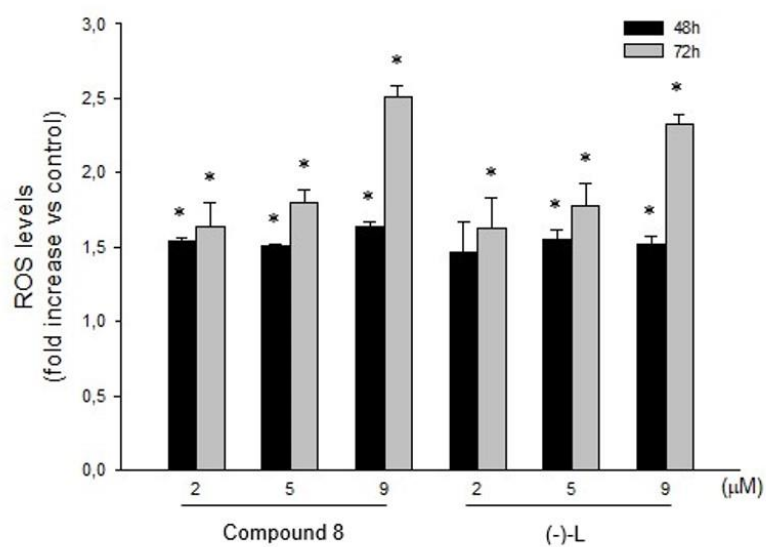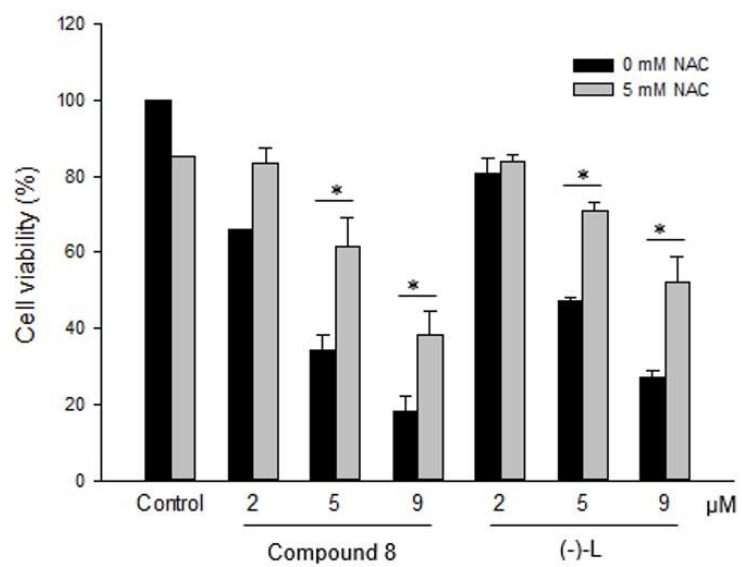
Graphical abstract

Table of contents entry
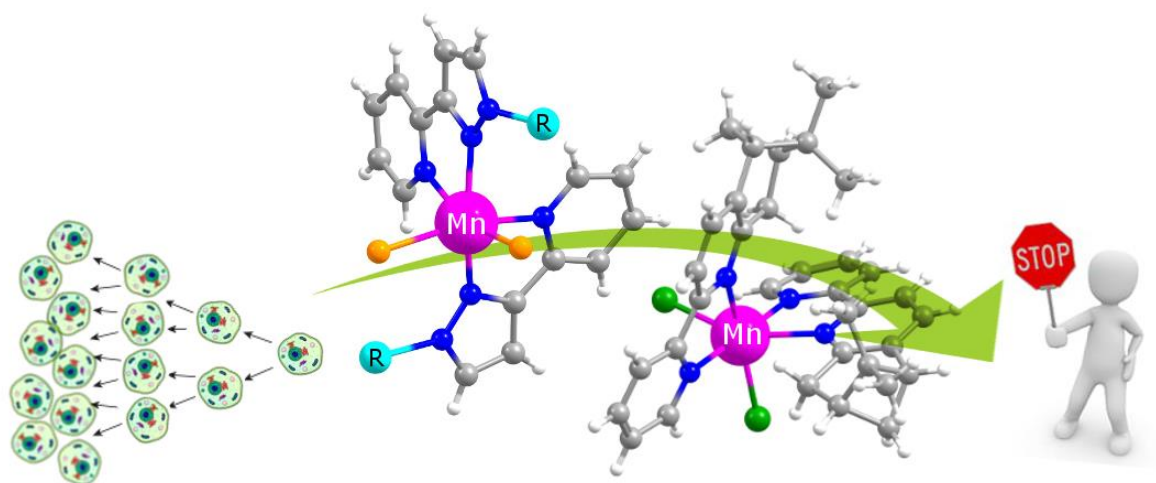
A new family of manganese compounds with cytotoxic activity have been synthesized and fully characterized. This work establishes the structure–activity relationships presented by the compounds tested.

Highlights

- The complex isomers influence their ability to interact with biomolecules
- Antiproliferative activity of compounds rises as hidrophobicity around Mn increases
- ROS generation allows compounds to cut the DNA